Doppler Velocity Recovery and Dealiasing Algorithm for Multi-PRT Scans in Weather Radars

David Schvartzman, *Senior Member, IEEE*, and Robert D. Palmer, *Fellow, IEEE*

***Abstract*— Pulsed Doppler radars are susceptible to range–velocity ambiguities inherent from using a uniform train of electromagnetic pulses to sample the atmosphere. Ambiguities arise due to the well-known Doppler dilemma, where increasing the pulse repetition time (PRT) increases the maximum unambiguous range but decreases the maximum unambiguous velocity and vice versa. Demands on any of the techniques to simultaneously mitigate these range-and-velocity ambiguities increase to a point of breakdown when they are needed most, that is, in the presence of widespread outbreaks of severe weather with convective storm over large areas. In this article, we present an algorithm to increase the region of valid Doppler velocities recovered when multi-PRT scans are used. The velocity recovery and dealiasing (VRAD) algorithm blends data from different scans and uses simple dealiasing techniques to mitigate regions with obscured velocity estimates. Data from the operational WSR-88D network are used to demonstrate the algorithm. On average, the algorithm is able to increase valid velocity estimates by 25.67% in conventional scans (i.e., nonphase coded) and 12.42% in phase-coded scans.**

***Index Terms*— Dealiasing, Doppler velocity, velocity recovery, weather radar.**

I. Introduction

THE Radar Operation Center (ROC) of the National Weather Service plays a pivotal role supporting Weather Surveillance Radar-1988 Doppler (WSR-88D). The radars provide crucial data to protect lives and property and of all U.S. Government-distributed data are the second highest used by public. The volume coverage patterns (VCPs) employed by the WSR-88D in precipitation mode include "split cuts" and phase-coded waveforms at low elevations [1], [2]. In split cuts, a specific elevation angle is scanned twice, utilizing two different pulse repetition times (PRTs)— resulting in two 360° azimuthal rotations of the antenna at the same elevation angle [3]. During the first half, referred to as the surveillance scan (CS scan), a long PRT produces spatial coverage without range ambiguities. In contrast, the second half, known as the Doppler scan (CD scan), employs a short PRT, which can be phase coded or not, to minimize the occurrence of velocity aliasing, increasing the maximum unambiguous velocity (v_a) at the expense of a shorter maximum unambiguous range (R_a) [4]. This approach enhances the coverage of weather surveillance with unambiguous velocity estimates. Split cut scans are used in the lower elevations of most WSR-88D VCPs, to mitigate range–velocity ambiguities.

These techniques effectively address range-and-velocity ambiguities, as outlined by the Office of the Federal Coordinator for Meteorology (OFCM) [5], [6]. The challenge in simultaneously resolving range and velocity ambiguities arises due to the coupling between R_a and v_a defined as follows [4]:

$$R_a = \frac{cT_s}{2} \quad \text{and} \quad v_a = \frac{\lambda}{4T_s} \tag{1}$$

where T_s is the PRT, λ is the radar wavelength, and c is the speed of light. Multiplying the expressions in (1) results in the "Doppler Dilemma"

$$R_a v_a = \frac{c\lambda}{8} \tag{2}$$

which shows the coupling between R_a and v_a. Since c is a constant and λ is typically a fixed parameter in a radar system, there is no direct way to simultaneously get high unambiguous range and velocity measurements. Moreover, demands on any of the mitigating techniques increase to a point of breakdown when they are needed most. That is, in widespread outbreaks of severe weather with convective storm over large areas, producing returns of excessive dynamic range, and large dispersion of Doppler velocities.

Operationally, reflectivity (Z_h), differential reflectivity (Z_{DR}), differential phase (Φ_{DP}), and copolar correlation coefficient (ρ_{hv}) are obtained from the CS scan, whereas Doppler velocity (v_r) and spectrum width (σ_v) are obtained from the CD scan and are "range unfolded" relying on the reflectivity from the CS scan [5]. While currently not used operationally, Doppler velocity estimates from the CS scan could be used to significantly extend the range where valid velocity estimates from the CD scan are not available. However, CS-scan velocities will likely present considerable aliasing, and the standard deviation of velocity estimates would most likely be larger than that of the CD-scan estimates. An analysis of the standard deviation of estimates would be required to evaluate the conditions in which CS-scan velocities could be blended with CD-scan velocities. Furthermore, the CS-derived velocities could be used to "dealias" velocities exceeding v_a in the CD scan. A similar concept, where redundant split cut data are used to improve polarimetric-variable estimates, is used in the hybrid scan estimators [3].

Manuscript received 13 March 2024; revised 1 May 2024; accepted 24 May 2024. Date of publication 28 May 2024; date of current version 10 June 2024. This work was supported by the School of Meteorology and the Advanced Radar Research Center, The University of Oklahoma. *(Corresponding author: David Schvartzman.)*

The authors are with the Advanced Radar Research Center (ARRC) and the School of Meteorology, The University of Oklahoma, Norman, OK 73019 USA (e-mail: dschvart@ou.edu; rpalmer@ou.edu).

Digital Object Identifier 10.1109/TGRS.2024.3406445

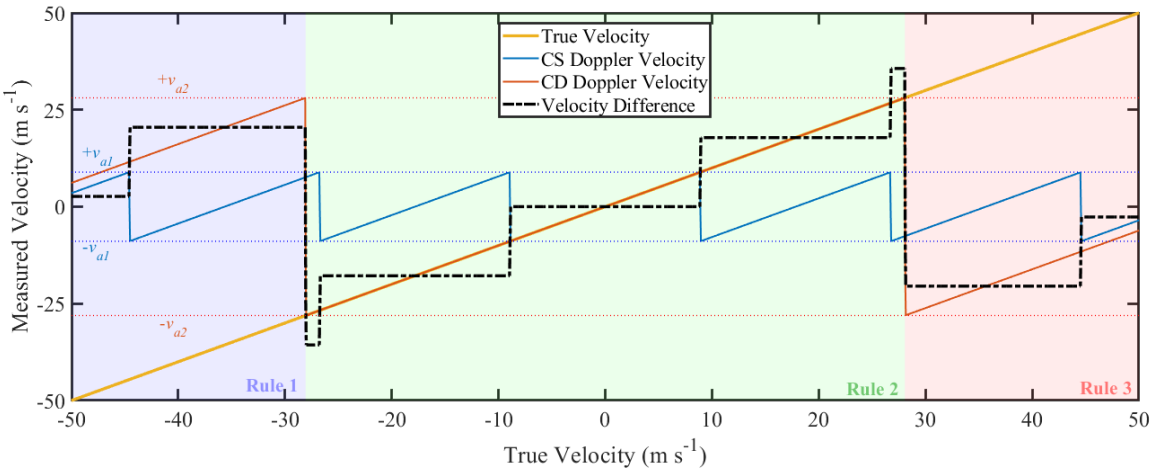

Fig. 1. Doppler velocities that would be measured with typical CS and CD scan parameters (in this case, those used operationally by the Houston, TX KHGX on 2017-08-27). The solid blue and orange curves show the CS and CD Doppler velocities and the corresponding dotted lines indicate the va_1 and va_2 boundaries, the yellow curve is the true velocity, and the dotted black curve is the difference in velocities.

In this article, we propose a simple yet effective algorithm designed to seamlessly integrate CS and CD data, thereby enhancing Doppler velocity estimates. The velocity recovery and dealiasing (VRAD) algorithm delivers improvements through two key mechanisms. First, in areas exhibiting valid CD estimates that are subject to aliasing (i.e., high velocities surpassing the Nyquist interval), the algorithm employs CS data to ascertain the aliasing ratio in CD velocities, facilitating unfolding and the recovery of appropriately dealiased Doppler velocity estimates. The proposed algorithms use a dual-PRT technique, whereby the two PRTs differ by a factor of approximately three and data are from two contiguous scans. In the common dual-PRT method, the two PRTs differ by a factor of about 30%–50% and are transmitted alternately in adjacent dwells (i.e., similar to the "batch mode" in the WSR-88D) [7], [8]. Similar techniques for dealiasing velocities using multiple scans have been proposed [9], [10], [11].

Second, it addresses the challenge of obscured velocities, a common occurrence in WSR-88D data where estimates are often obscured, indicated as "RF—range folded" (depicted in purple hues), especially at range locations featuring multiple overlaid velocity estimates. In such instances, the algorithm uses CS-scan velocities to populate the otherwise inaccessible or obscured velocity regions, enhancing data availability. This is the most important contribution of the manuscript—the recovery of otherwise unrecoverable (or obscured) Doppler velocity estimates. It is noted that describing RF estimates as "range folded" is incorrect, since they are not folded. The estimates are correctly placed, as the range unfolding algorithm determines their correct location. However, these estimates contain *overlaid* returns, coming from ranges spaced by the maximum unambiguous range. Hereafter, the acronym RF is used, considering that it is the official terminology defined in the interface control document of the WSR-88D data; however these should be interpreted as range-overlaid returns. In summary, this algorithmic approach enhances the availability of Doppler velocity estimates (otherwise censored).

The article is organized as follows. Algorithm descriptions and simple simulations for the dealiasing and echo recovery techniques are provided in Section II. An experimental demonstration using archived data from the WSR-88D is presented in Section III. Cases including conventional split cuts (i.e., no phase coding) and phase-coded split cuts are presented. Algorithm performance is discussed in Section IV. The number of recovered Doppler velocity estimates and their associated spatial extent is computed to quantify the advantages of the proposed algorithm. Limitations are also discussed in Section IV. A summary is provided in Section V.

II. Algorithm Description and Implementation

Two techniques are developed to improve the dealiasing and recovery of Doppler velocity estimates. The dealiasing technique draws from principles used in both the staggered PRT (SPRT) [12] and 2-D velocity dealiasing (2DVDA) [13] algorithms. The recovery technique uses likely aliased CS velocity estimates to recover otherwise obscured velocities in the CD scan. A boundary condition that ensures a continuous velocity transition from the valid CD estimates to the potentially aliased CS estimates in the RF region is applied to determine the number of aliases (to add or subtract multiples of $2v_a$) and to dealias these CS velocities. Then, velocities recovered from the CS scan are used to populate the obscured regions in the field of velocities derived from the CD scan.

A. Dealiasing

When Doppler velocity measurements exceed the maximum unambiguous velocity, aliasing occurs, and apparent velocities are incorrect. This can be expressed by

$$v_r = v_T \pm 2\, k v_a \tag{3}$$

where v_r is the measured apparent Doppler velocity, v_T is the true Doppler velocity, and k is an integer that represents

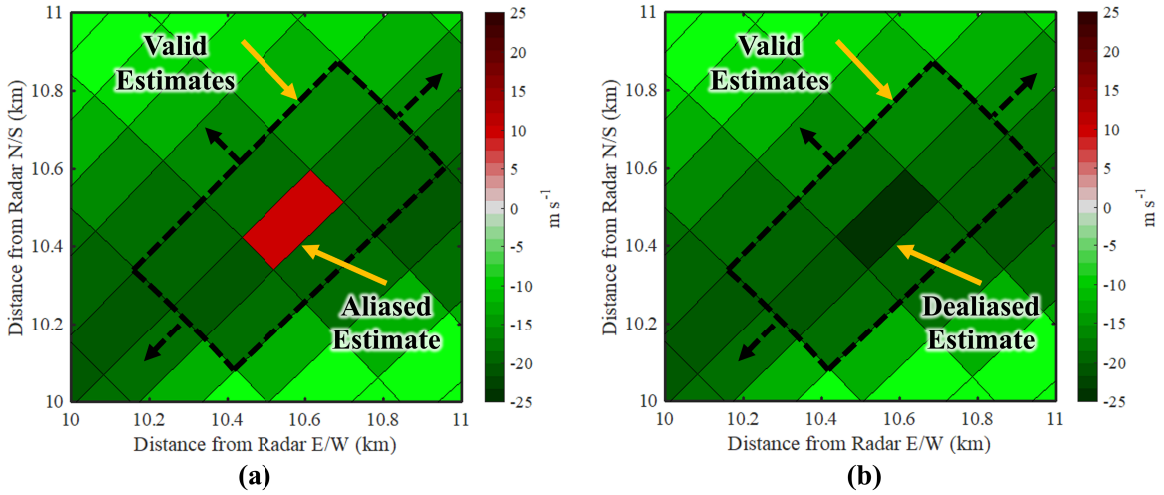

Fig. 2. Median filter dealiasing concept, where (a) has an aliased velocity prior to the application of the filter and (b) shows the dealiased velocity. The black dotted line represents the boundaries of the filter, in this case a 3 × 3 local neighborhood, and the arrows indicate that it is a running window that moves across the entire Doppler velocity field.

the number of times velocities were aliased in the Nyquist interval ($2v_a$). Given the different PRTs used in the CS and CD scans, aliasing velocities from these scans differ. These can be calculated with (1), and the corresponding unambiguous velocities are defined as v_{a1} for the CS, v_{a2} for the CD, and naturally $v_{a2} > v_{a1}$.

The proposed dealiasing algorithm is implemented as a two-stage process. The first stage leverages the different unambiguous velocities resulting from different PRTs, and follows a traditional approach as that used in the SPRT algorithm. The second stage leverages the spatial continuity of Doppler velocity measurements and uses a 2-D median filter. Next, we describe the stages.

1) Velocity Difference Dealiasing: The difference between Doppler velocity measurements produces a characteristic graph that can be used to estimate dealiased velocities. This dealiasing scheme is similar to that described in the SPRT algorithm. Fig. 1 shows Doppler velocities that would be measured with typical CS and CD scan parameters. Parameters used for this example are as those on the operational KHGX radar in Houston, TX, during the Harvey Hurricane (2017-08-26). The radar frequency was 2.7050 GHz, and the CS and CD PRTs were 3.1067 ms and 0.9866 ms. The dotted black curve is the difference in velocities, CD–CS, where parts of constant differences at different levels can be seen. These differences are used to estimate which velocity is correct. For this specific case with KHGX velocities, the dealiasing rules based on the characteristic velocity difference ($v_d = v_{r2} - v_{r1}$) are as follows (see colored regions in Fig. 1).

1) *Rule 1:*
   a) $v_d \approx 2.6508 \pm \varepsilon$ ms^{-1}, then $v_T = v_{r2} - 2v_{a2}$, or
   b) $v_d \approx 20.4835 \pm \varepsilon$ ms^{-1}, then $v_T = v_{r2} - 2v_{a2}$.
2) *Rule 2:*
   a) $v_d \approx -35.665 \pm \varepsilon$ ms^{-1}, then $v_T = v_{r2}$, or
   b) $v_d \approx -17.8325 \pm \varepsilon$ ms^{-1}, then $v_T = v_{r2}$, or
   c) $v_d \approx 0$ ms$^{-1} \pm \varepsilon$, then $v_T = v_{r2}$, or
   d) $v_d \approx 17.8325 \pm \varepsilon$ ms^{-1}, then $v_T = v_{r2}$, or
   e) $v_d \approx 35.665 \pm \varepsilon$ ms^{-1}, then then $v_T = v_{r2}$.
3) *Rule 3:*
   a) $v_d \approx -20.4835 \pm \varepsilon$ ms^{-1}, then $v_T = v_{r2} + 2v_{a2}$, or
   b) $v_d \approx -2.6508 \pm \varepsilon$ ms^{-1}, then $v_T = v_{r2} + 2v_{a2}$

where v_{r1} and v_{r2} are the measured velocities in the CS and CD scans, and ε is a parameter to extend the range of velocities satisfying each rule. This parameter is needed, because in practice, Doppler velocity measurements exhibit unavoidable estimation errors, and thus, ideal identities are ineffective. Previous research on SPRT provides expressions to calculate optimal ε [14], although these are not implemented here. In the proposed VRAD algorithm, a value of $0.25v_{a1}$ is adopted, and while it may not be optimal, it does produce sufficiently large regions of correctly dealiased velocities so that the next step in the dealiasing process can correct remaining estimates. Next we present another dealising technique more robust to "catastrophic errors" that can result from the SPRT algorithm, which is used in the VRAD algorithm.

2) Median Filter Dealiasing: The second stage of the proposed algorithm implements a velocity dealiasing methodology based on a 2-D median filter similar to 2DVDA. The core principle behind this dealiasing technique involves leveraging the spatial continuity of Doppler velocity measurements to identify and adjust values that are likely aliased. By comparing each velocity estimate against a dynamically calculated median value within a defined neighborhood, the algorithm identifies aliased velocities. If the difference between the velocity estimate under question and the local median velocity is greater than a set threshold, it is deemed as aliased. When an aliased velocity is found, multiples of $2v_a$ (e.g., $\pm 2, 4, 6$ v_a) are added to it and compared against the local median. Then, the value that results in the lowest difference against the local median is selected. This maintains the integrity of the original data structure, ensuring that corrected velocities remain consistent with surrounding measurements. Fig. 2 illustrates the concept, where a single aliased velocity is found in the running window. The median filter then dealiases by subtracting 2 v_a.

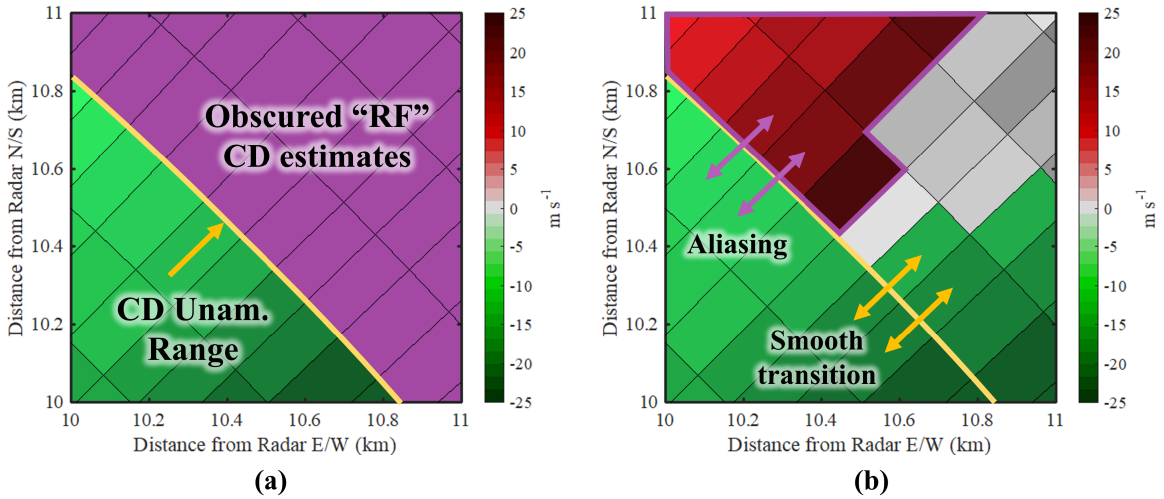

Fig. 3. Conceptual depiction of the velocity recovery technique, where (a) shows a field of CD velocities that has regions with obscured returns past the unambiguous range boundary, and (b) shows the field of CD velocities with the obscured RF region populated with potentially aliased CS velocities.

The performance of this dealiasing technique depends on the size of the running window. For larger areas with aliased velocities, larger running windows are needed. And since the size of the region with aliased velocities depends on the type of precipitation system (e.g., small in a supercell and large in a hurricane), the median-filter dealiasing technique is applied multiple times with different window sizes. This is needed because radars intrinsically sample the atmosphere in a polar coordinate system. Thus, fixed-size running median filters result in different effective areas as they move through the polar grid. Median filter sizes were evaluated empirically, and three sizes that resulted in best performance were selected. In this article, we use a set of fixed window sizes; however, window sizes could be selected dynamically based on the size of aliased velocity regions. That ensures robustness to different type of storms, although it is more computationally expensive.

B. Velocity Recovery

The most important contribution of this article is the echo recovery technique. The technique is conceptually and computationally simple and it can provide major value to operational meteorologists, in particular, to the US NWS forecasters. It can be applied in the split cut scans.

It consists of using the likely aliased CS-scan velocities (due to low v_a) to populate velocities in CD regions censored due to overlay in range (the so-called "purple haze" in radar data displays) and recover more Doppler velocity estimates. This is illustrated in Fig. 3. First, censored regions deemed as RF in the CD velocity field (i.e., overlaid returns) are extracted [Fig. 3(a)]. Then, CS velocities from those regions are used to create a hybrid CS/CD field of Doppler velocities. The valid CD velocities are kept, and only the RF regions are populated with CS velocity estimates [Fig. 3(b)]. Then, a simple 1-D dealiasing function is applied across the CS/CD boundaries considering that the CD estimates as correct (i.e., dealiased). The linear dealiasing function is defined as follows:

$$v_u = v_{r2} + 2\,p\,v_{a1} \tag{4}$$

where v_u is the dealiased CS velocity and p is an integer. As done before for the median filter dealiasing, p is the integer that minimizes the difference between v_u and v_{r2}. The key assumption is that the transition should result in a smooth field of Doppler velocities, expected from the physics of an atmospheric precipitation system. The linear dealiasing is applied following a spiral pattern in the CS-populated velocity regions, starting from a boundary between the CS and CD data, and moving inward. That is, the CD velocities are assumed to be correctly dealiased and the spiral dealiasing starts by comparing them to CS velocities along the CS/CD boundaries. After the CS velocities adjacent to CD estimates have been dealiased (the outer ring), the spiral dealiasing moves inward to the center of the RF region. If a velocity estimate extracted from the CS scan and placed in an RF region does not have a neighbor with a valid CD velocity (i.e., outer edge of precipitation system), the function skips that sample. As the function iterates over the region, skipped samples are eventually reached. This CS velocity dealiasing could be implemented in several ways, but following a spiral pattern was found to be the most robust method.

C. Dealiasing and Recovery Algorithm

The techniques described are combined as building blocks for the overall VRAD algorithm. The algorithm flowchart is shown in Fig. 4.

First, the range-unfolded field of CD Doppler velocities is passed as an input and instances for velocity aliasing are checked. If velocity aliasing is present, then the velocity difference and median filter dealiasing techniques described are applied. For the median filter dealiasing, three window sizes are used 5×5, 10×10, and 30×30. The smaller windows correct speckle-like aliased velocities and the larger

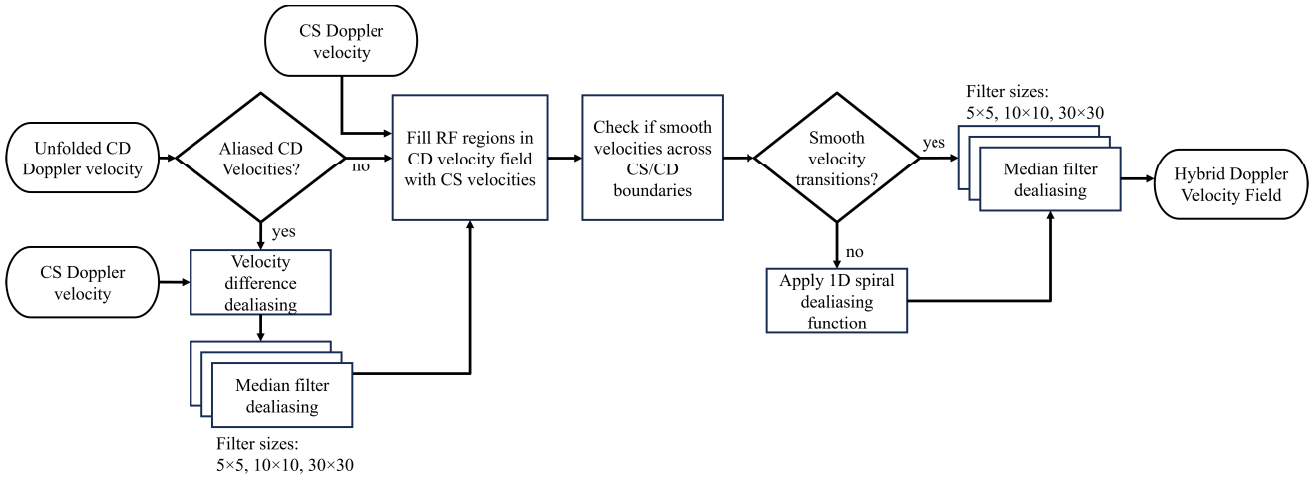

Fig. 4. Flowchart of the VRAD algorithm.

windows correct larger regions of aliased velocities.[1] After the dealiasing steps or if no velocity aliasing was present, the RF regions in the CD velocity field are populated with CS velocities. Then, CS/CD velocity transitions are checked for smoothness. In the current implementation, a threshold of 5 ms^{-1} is used to determine if the transition is smooth.[2] That is, if the velocity difference from a CD gate to a CS gate is less than 5 ms^{-1}, it is considered smooth or nonaliased. If the difference is greater than or equal to 5 ms^{-1}, it is considered aliased. The linear dealiasing function is applied on regions with nonsmooth transitions following a spiral pattern. Finally, the median filter dealiasing technique is applied to the hybrid Doppler velocity field to ensure no other instance of velocity aliasing is present.

III. Experimental Demonstration

The proposed algorithm is demonstrated by processing time-series in-phase and quadrature (IQ) data from WSR-88D systems using both the conventional and the VRAD algorithm. Herein, we present the results for three relevant cases: one case from a conventional scan and two from phase-coded scans.

A. Conventional Scan

Conventional scans are defined here as those in which neither the CS nor CD scans have pulse-to-pulse phase coding applied. That is, the time-series data in the CS and CD scans is collected with nonphase-coded pulse sequences at constant PRTs. These are typically used in "clear air" mode and for relatively weak precipitation events (e.g., snowstorms and ice storms) because they use a high number of pulses in the CD scan, which improves data quality.

On December 13, 2020, a winter storm warning was issued covering most of north and central Oklahoma. Moderate to heavy snowfall blanketed parts of Oklahoma. Approximately 3 in of snow accumulation was reported on average with some higher accumulations up to around 6 in in north and west of Oklahoma City. There were several power outages and road closures.

Time-series IQ data collected by the KCRI WSR-88D radar in Norman, OK at approximately 21:54:49 UTC was processed to evaluate the VRAD algorithm. The radar was running the operational VCP 32, typical for widespread precipitation systems that produce overall weak signal-to-noise ratio (SNR). The PRT used for the CS scan was 3.066 ms and 67 samples were collected per dwell. The PRT used for the CD scan was 0.973 ms and 227 samples were collected per dwell. With this, the CS and CD maximum unambiguous velocities are $v_{a1} = 9.03$ ms^{-1} and $v_{a2} = 28.47$ ms^{-1}. Processed fields of radar data are shown in Fig. 5, where the black dot represents the radar location. The radar reflectivity field (top-left panel) is included for reference to provide storm context. The CD velocity field shows what the WSR-88D currently provides with the operational algorithm. Large regions with overlaid returns (i.e., the RF or purple haze) are present to the southwest and east of the radar, where velocity estimates are overlaid from the first and second trips of the CD pulses. The bottom-left panel shows the CS velocity field, where velocity aliasing is more evidently present to the north and south of the radar and also near the outer edges of the storm.

After applying the VRAD algorithm, the bottom-right field of velocity estimates is produced. Since there were no aliased velocities in the CD scan, the initial velocity difference and median filter dealiasing were not needed. A smooth transition past the unambiguous range of the CD scan is observed, where changes in the field of Doppler velocity across the boundary are <5 ms^{-1}. A region with overlaid returns close to the radar in the CD scan is recovered by the VRAD algorithm as shown in Fig. 6. It can be seen that in the region with overlaid returns, velocities are completely recovered using the VRAD algorithm, which provides a smooth field of Doppler velocities. A total of 1 03 940 velocity samples from obscured range locations were recovered, which represents 26.55% of the valid meteorological returns in this case. These cover an area of approximately 38 000 km^2.

[1]Filter sizes are adjustable parameters that can be changed for systems with potentially different aliased-velocity regions.

[2]This parameter was chosen based on current cases evaluated; however, it can be changed to optimize algorithm performance.

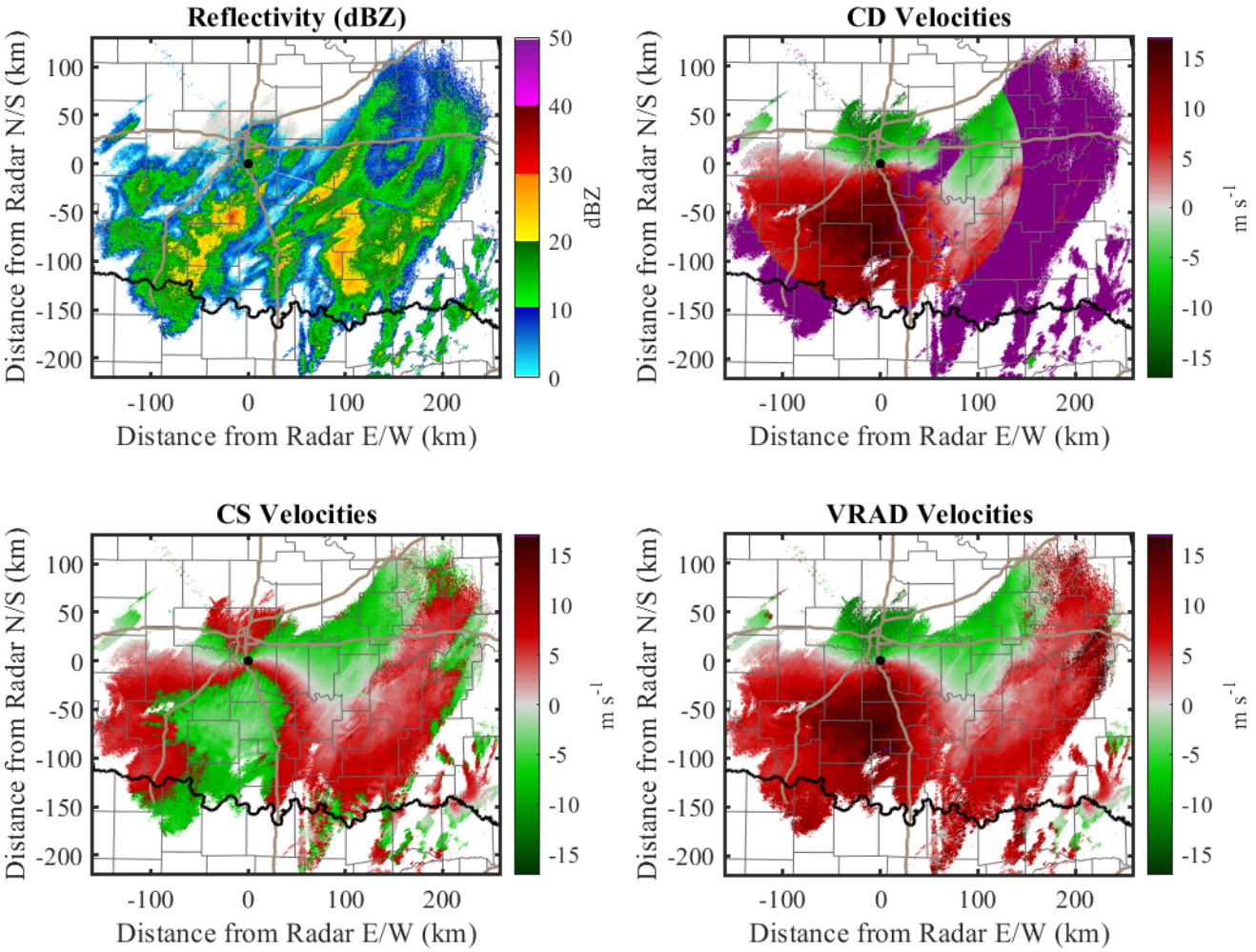

Fig. 5. Snowstorm event in OK on December 13, 2020, observed by the KCRI WSR-88D radar at approximately 21:54:49 UTC. The reflectivity field (top-left) is included for reference. The CD velocity field (top-right) is the field of velocity estimates currently provided by the WSR-88D. The black dot represents the radar location. State boundaries are indicated in bold black, counties are in gray lines, and roads are indicated in gold lines.

B. Phase-Coded Scans

Volume coverage patterns with phase-coded scans are typically used in convective precipitation modes. Phase coding the transmit pulses enables significant mitigation of range–velocity ambiguities [2], [15]. In the Sachidananda and Zrnić-2 (SZ-2) phase coding technique operational on WSR-88Ds, transmitted pulses are phase shifted according to a sequence referred to as the switching code. The received echo samples are multiplied by the conjugate of the switching code sequence to remove the phases of transmit pulses artificially imposed by the switching code. Consequently, the first trip signals are made coherent and second (or higher order) trip signals are phase modulated. In general, any one of the overlaid trip signals can be cohered leaving the rest modulated by different codes. This allows the recovery of Doppler velocity measurements beyond the theoretical maximum unambiguous range in the CD scan. Given the extended range of valid Doppler velocities recovered with phase-coded scans, these are typically used for observing precipitation.

1) Harvey Hurricane: On August 26, 2017, the devastating Harvey Hurricane had made landfall on the coast of Houston, TX. It was rated as category 4 in the Saffir–Simpson scale, indicating that the 1-min maximum sustained winds were in the range from 58 to 70 ms^{-1}. These maximum wind speeds greatly exceed the typical maximum unambiguous velocities that weather radars can measure; therefore, aliasing is expected. Harvey caused catastrophic flooding, more than 100 deaths and major economic impacts to the region (estimated total damage at $125 billion[3]). The resulting floods inundated hundreds of thousands of homes, which displaced more than 30 000 people and prompted more than 17 000 rescues. The storm also spawned approximately 53 tornadoes across six states.

Time-series IQ data from the operational KHGX observing the Harvey Hurricane at approximately 02:17:36 UTC was acquired[4] to evaluate the proposed VRAD algorithm. The radar was running the operational VCP 212, which uses a PRT of 3.1067 ms with 16 samples per dwell in the CS scan, and a PRT of 0.986 ms with 64 samples in the CD scan.

[3]Source: "Costliest U.S. tropical cyclones tables updated" by NOAA's National Hurricane Center, available here: https://www.nhc.noaa.gov/news/UpdatedCostliest.pdf.

[4]Available at: https://www.ncei.noaa.gov/acce ss/search/data-search/nexrad-level-1-event-data.

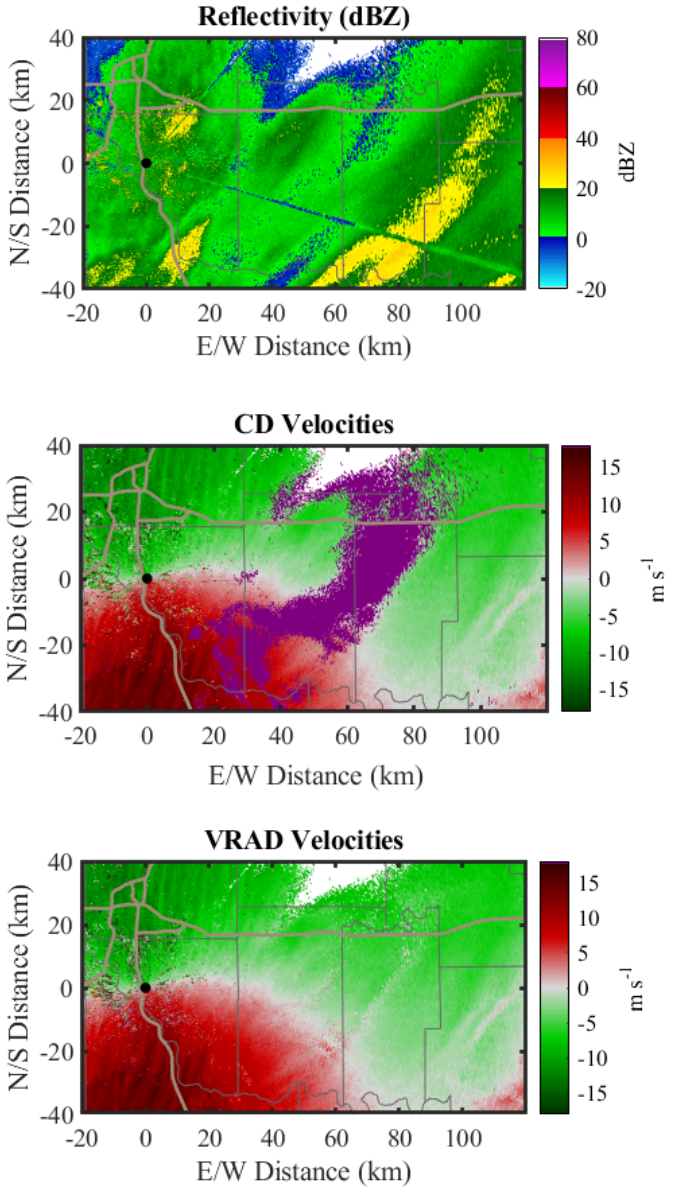

Fig. 6. Same as Fig. 5, but zoomed in the region with overlaid returns east of the radar.

These result in maximum unambiguous velocities of $v_{a1} = 8.92$ ms^{-1} and $v_{a2} = 28.08$ ms^{-1}. Processed fields of radar data are shown in Fig. 7, where the black dot represents the radar location. Panels are organized as in Fig. 5. The top-right panel shows the CD velocities produced by the WSR-88D real-time processing. It can be seen that the measurements around the eye of the hurricane are aliased and are entirely recovered by the SZ-2 processing algorithm in the second trip (i.e., past the maximum unambiguous range of the CD scan). Rings of RF-marked data are seen at ranges of approximately 150–300 km. These correspond to range-overlaid returns that cannot be resolved by the SZ-2 algorithm, usually caused by strong ground clutter near the radar. The bottom-left panel shows the CS velocities, which are aliased several times due to the low v_{a1}.

The bottom-right panel shows the field of velocity estimates produced by the VRAD algorithm. In this case, the velocity difference and median filter dealiasing techniques were applied to the CD data, before the velocity recovery technique. The resultant field of velocities appears to be dealiased correctly and does not show regions with range-overlaid (purple hues) echoes after applying the velocity recovery (bottom-right panel in Fig. 7). That is, all censored velocity estimates were recovered using the CS-scan data and the boundary conditions applied with the echo recovery technique. This is especially important in large and impactful precipitation systems like the Harvey Hurricane, because several potentially tornadic circulations can span on the edges of the hurricane and be obscured by overlaid returns. We note that dealiasing velocities in large regions, such as those around the eye of a hurricane, are typically challenging, and techniques such as the velocity difference dealiasing can be beneficial. Fig. 8 shows a close-up view of the Z_h (reference), CD-scan v_r, and VRAD v_r fields. In the VRAD field, it can be seen that the circular artifact created by range-overlaid returns of ground clutter is mitigated and recovered values produce smooth velocities. A total of 45 645 velocity samples from obscured range locations were recovered, which represents 10.24% of the valid meteorological returns in this case. Velocity data covering an area of approximately 20 000 km^2 was recovered.

2) Severe Weather Outbreak: A severe weather outbreak took place on August 7, 2023 across parts of the eastern U.S., stretching from Georgia to New York. Widespread and locally destructive damaging winds and tornadoes were the greatest threats. Millions of people were placed under tornado and severe thunderstorm watches as powerful thunderstorms brought flooding rain, hurricane-force wind gusts, large hail and tornadoes in the evening hours. The storms left more than a million homes and businesses without power and grounded hundreds of flights.[5] There were 16 confirmed tornadoes reported: 4 EF-0, 11 EF-1, 1 EF-2, and 1 EF-3 (EF is the Enhanced Fujita scale). Two fatalities were reported.

Time-series IQ data from the operational KLWX in Sterling, VA observing the severe weather outbreak at approximately 22:06:21 UTC was acquired to evaluate the proposed VRAD algorithm. As in the previous case, the radar was running the operational VCP 212, which uses a PRT of 3.1067 ms with 16 samples per dwell in the CS scan, and a PRT of 0.986 ms with 64 samples in the CD scan. Since v_a depends on the radar frequency, the maximum unambiguous velocities for this case are slightly different, $v_{a1} = 8.17$ ms^{-1} and $v_{a2} = 25.74$ ms^{-1}. Processed fields of radar data are shown in Fig. 9, in a layout similar to previous examples. Evaluating the CD-scan velocities (top-right panel), it is apparent that storms were moving at high speeds, and some areas of aliasing to the east and west of the radar can be seen. In this case, velocity aliasing has some overlap on regions with overlaid returns, which means that data from rapidly evolving severe storms was obscured. At approximately 120 km east and 85 km north of the radar, a "bow echo" with a core of high Z_h can be seen moving SW to NE. A broad circulation signature

[5]Sources: NOAA, "Billion Dollar Climate Disasters" https://www.ncei.noaa.gov/access/billions/events.pdf and The New York Times, article "Cleanup Begins After Severe Storms Tear Through Eastern U.S.," https://www.nytimes.com/2023/08/08/us/us-severe-storms-damage.html.

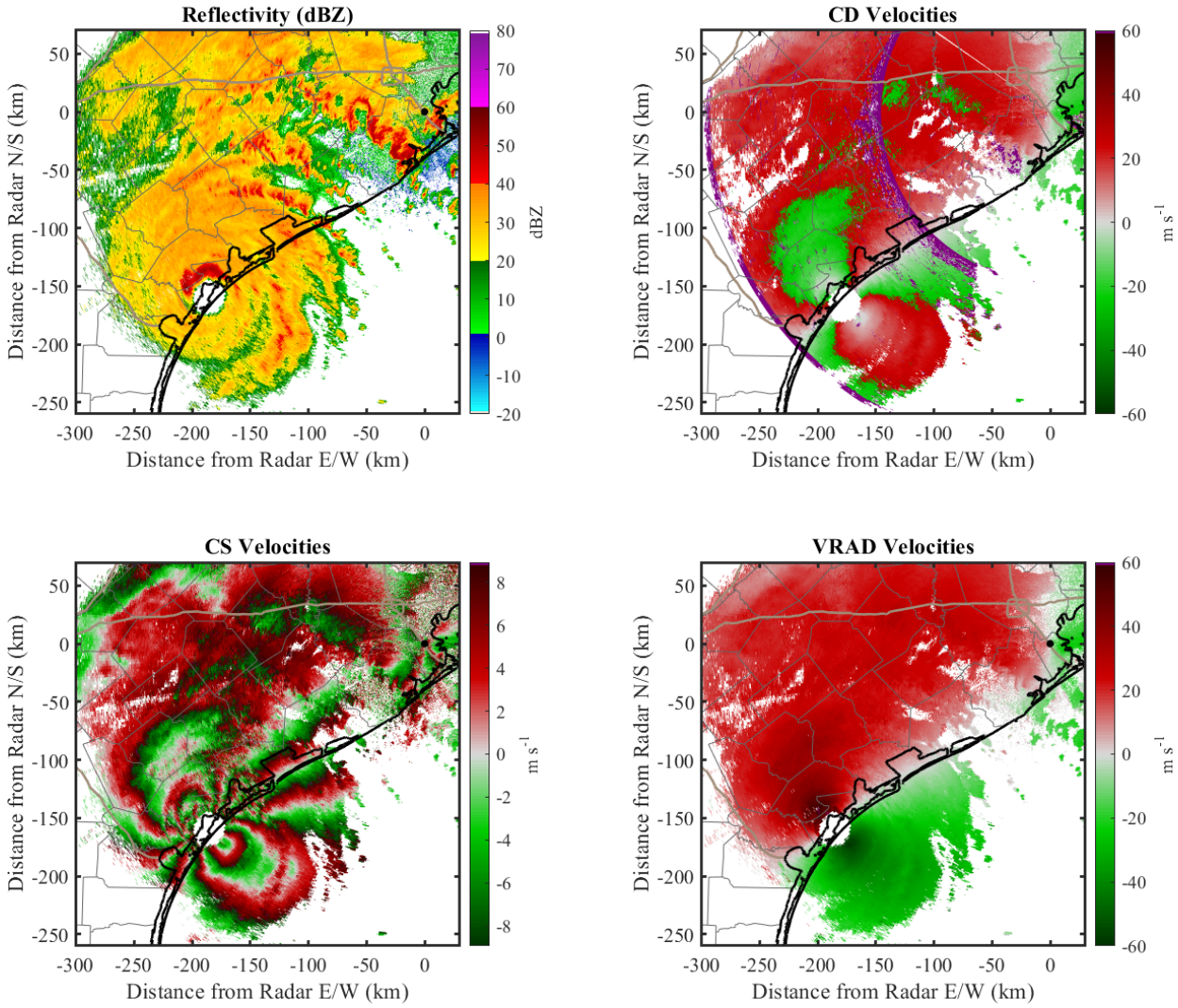

Fig. 7. Similar to Fig. 5, but for the Harvey Hurricane, which devastated the city of Houston, TX in 2017. Data was collected with the operational KHGX radar on August 26, 2017, around 02:17:36 UTC.

(i.e., red to gray to green) is obscured by a circle of range-overlaid returns. Severe thunderstorm warnings were in effect during this time, and NWS forecasters stated that "Radar has indicated rotation within these severe thunderstorms. Although a tornado is not immediately likely, tornadoes can develop quickly during severe thunderstorms." Forecasters and radar operators normally have the ability to select different PRTs to shift the circle of range-overlaid returns when it obscures important regions in the CD scan. However, in certain severe weather scenarios like this one, it is challenging to avoid range-overlaid returns on significant storm regions, since severe storms are widespread. In these cases, recovering velocities in the region with range-overlaid returns is of critical importance.

The bottom-right panel shows the field of velocity estimates produced by the VRAD algorithm. As in previous cases, it is apparent that the VRAD algorithm produces a smooth field of dealiased velocities, mitigating regions with range-overlaid returns. In addition to eliminating the circle of range-overlaid returns near the end of first trip signals, the VRAD algorithm recovers otherwise obscured velocities beyond the second trip. This can be seen in the top-right corner, approximately 300 km north and 200 km east of the radar. Fig. 10 shows a close-up view of the Z_h (reference), CD-scan v_r, and VRAD v_r fields. The most important observation is the recovery of velocities revealing a broad circulation, approximately 120 km north and 100 km east of the radar. The circulation is evident by the reduction in the values of outflow velocities (red tones), their transition to near-zero velocities (gray tones), and even low inbound velocities (green tones). This structure is consistent with the bow echo observed in the Z_h field. Additionally, this case was selected because it illustrates a situation where the VRAD algorithm fails in correctly recovering all velocities. This can be seen near the bottom-right corner (80 km north, 140 km east), where the velocity transitions do not appear to be smooth (i.e., contrasting darker red tones). This happens due to the occurrence of velocity aliasing in the CD scan concurrent with the region with range-overlaid returns, which makes correct recovery and dealiasing more challenging. Limitations of the algorithm will be discussed in Section IV, and a

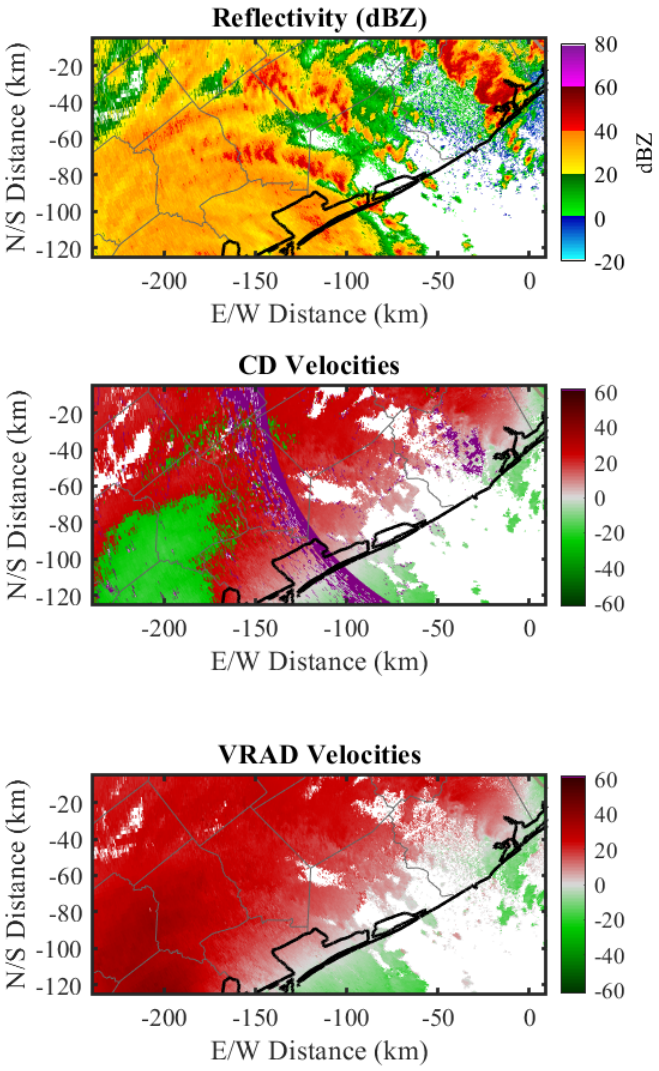

Fig. 8. Same as Fig. 7, but zoomed in the region with range-overlaid returns west of the radar.

metric for evaluating incorrectly dealiased regions will be introduced. A total of 35 128 velocity samples from obscured range locations were recovered, which represents 10.56% of the valid meteorological returns in this case. Velocity data covering an area of approximately 14 400 km^2 was recovered.

IV. Performance Evaluation

In this section, we quantify the improvement provided by the VRAD algorithm in two ways. First, we conduct time-series IQ data simulations for different signal parameters, to quantify the standard deviation of VRAD velocity estimates. Afterward, we apply the algorithm to ten cases from the WSR-88D and use metrics to quantify its performance.

A. Time-Series Simulations

We use simulations to compare the statistical performance of Doppler velocity estimates from the CS and CD scans at the lowest elevation angle, using parameters from operational VCPs (12 and 212). Simulations are conducted following the method proposed by [16]. For the VCP 12 simulations, the CS-scan PRT is $T_s = 3.12$ ms ($v_a = 8.32$ ms^{-1}) with $M = 15$ samples per dwell, and the CD-scan PRT is $T_s = 0.986$ ms ($v_a = 26.24$ ms^{-1}) with $M = 40$ samples per dwell. For each simulation, we generate 1 00 000 realizations of weather-like IQ signals varying the SNR from 2 to 20 dB in 0.5 dB steps. Simulations are generated for three values of σ_v, namely, 1, 2, and 4 ms^{-1}. For the estimation of Doppler velocities, we use the conventional lag-1 autocorrelation estimator [4]. The Von Hann window was applied to the time-series data to emulate the WSR-88D Doppler velocity processing [17]. Since the velocity estimator is unbiased, we set the true velocity to 0 ms^{-1} without loss of generality.

The standard deviation of simulated Doppler velocity estimates are presented in Fig. 11. Results obtained for the acquisition parameters of VCP 12 are shown on the left column, and those for VCP 212 are shown on the right column. From top to bottom, the rows present results for different σ_v values (1, 2, and 4 ms^{-1}). Solid black lines represent the standard deviation of CS estimates, dashed lines represent those for the CD estimates, and orange lines are the absolute differences between the CS and CD standard deviation curves. Note that the absolute error lines are referenced with the right ordinate axis. Results show that CD-scan velocities have lower standard deviation of estimates in general, except at low SNRs, with $\sigma_v = 1$ ms^{-1}, for the parameters in VCP 12 (top-left plot). This is expected, since the CD scan uses a considerably higher number of samples.

The required precision of estimates for the WSR-88D is less than or equal to 1 ms^{-1} for returns with a true spectrum width of 4 ms^{-1} and SNR $>$ 8 dB (WSR-88D System Specifications, ROC). This is the case for both CS and CD scans as seen in the top four plots in Fig. 11. As the spectrum width increases to 4 ms^{-1}, the absolute differences between CS and CD scans become considerably larger. Therefore, the standard deviation of velocity estimates, in CS scans, exceeds the requirements for the WSR-88D. The increased standard deviation leads to noisier velocity estimates which results in a higher number of "catastrophic errors." The latter occurs in the dealiasing process, using CS and CD velocities, whereby the difference of the two estimates maps the dealiased velocity to an incorrect region on the difference map (i.e., the dashed line in Fig. 1). This is because the variance of the difference is the sum of variances of the two estimates. Consequently, as the noisiness of this difference becomes larger (e.g., at $\sigma_v = 4$ ms^{-1}), the dealiasing process fails more often. This effect is exacerbated when the difference map has regions with flat levels that exhibit small differences. It should be noted, though, that the median σ_v in stratiform rain and snow, and isolated tornadic storms is less than 2 ms^{-1} [18]. Thus, assuming equal distribution of velocities around the median, it may be conjectured that at least ~50% of velocities are conducive to reliable dealiasing using CS and CD scans given sufficient separation among flat levels in the difference map (e.g., as in Fig. 1). Furthermore, enabling technology that can significantly reduce the standard deviation of estimates exists, and is currently being considered for implementation in the WSR-88D network. Specifically, the range-oversampling and whitening algorithm [19] would significantly reduce the

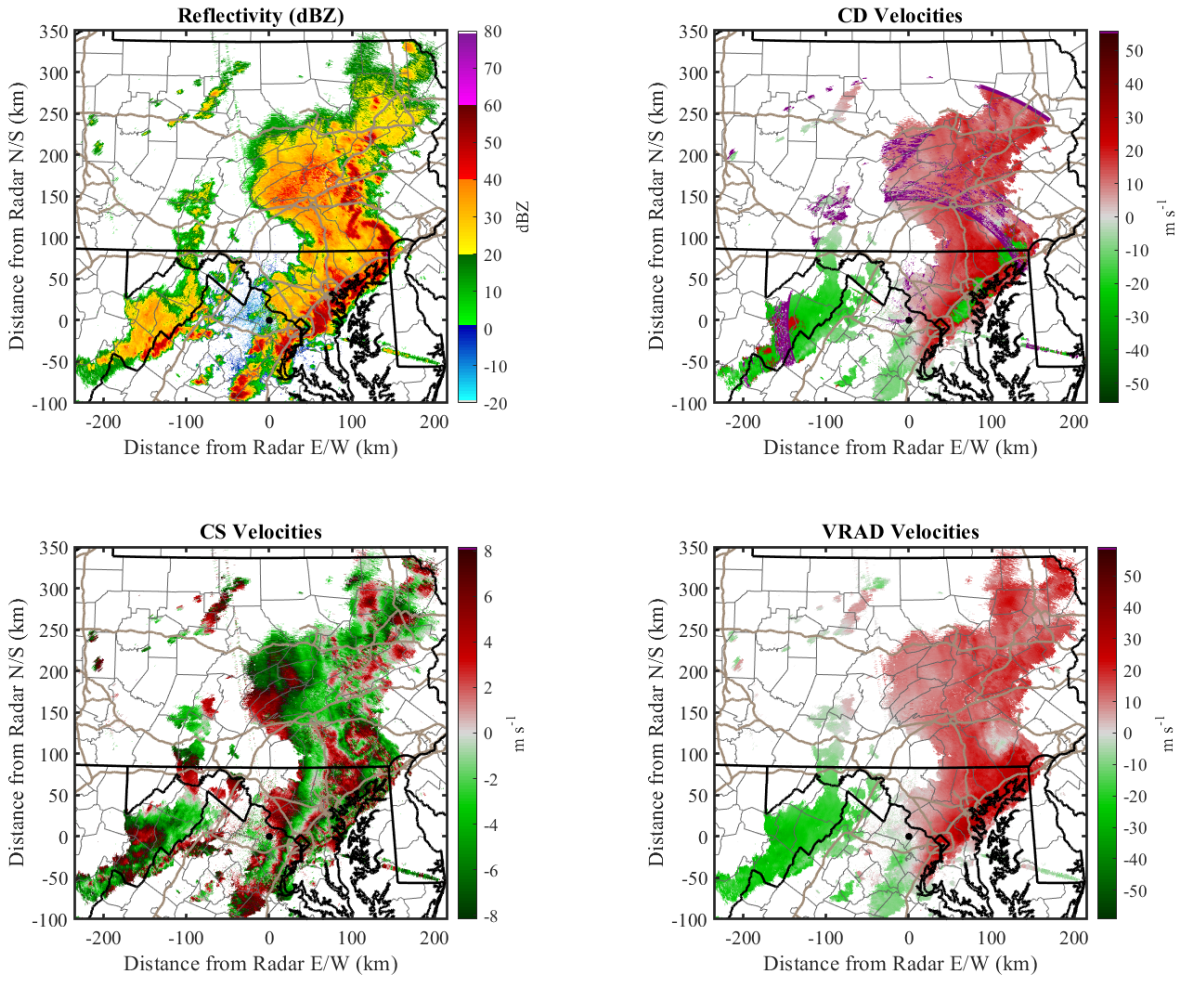

Fig. 9. Similar to Fig. 5, but for the severe weather outbreak that devastated North-East US in August 2023. Data was collected with the operational KLWX radar on August 7, 2023, around 22:06:21 UTC.

standard deviation of both CS and CD extracted velocity estimates in VRAD, thus improving the velocity dealiasing process.

Given the above considerations, an operational implementation may involve a setup where radar operators and forecasters could have the option to toggle between CD and VRAD estimates.

B. Weather Radar Observations

The VRAD algorithm performance is evaluated processing a total of 10 cases from various types of precipitation systems (i.e., convection, winter precipitation, and widespread stratiform), and considering certain metrics. First, the total number of velocity estimates recovered is quantified. That is, the number of recovered RF-designated velocities from obscured range locations (in purple hues) is counted. Next, the total area of these regions is computed. Finally, the number of range gates on which the algorithm fails is estimated. Failed velocity recoveries are those that exhibit a nonsmooth transition to at least one of the neighboring estimates. A threshold of 5 ms^{-1} is selected because it is approximately one-half of the average maximum unambiguous velocity in the CS scan. This rule works well for the cases analyzed. However, it may not be effective when strong and tight velocity couplets are present (e.g., tornadic circulations), since velocities in adjacent gates can differ by more than 5 ms^{-1} in those cases. Determining when velocity aliasing occurs is challenging in general; however, it is not critical to evaluate the VRAD algorithm. The key contribution in the VRAD algorithm is in the use of CS velocities to populate otherwise obscured CD velocities. Velocity dealiasing was necessary to accomplish this, but other existing dealiasing algorithms (e.g., [13], [20], [21]) could be used instead.

The performance metrics are presented in Table I, where cases evaluated are sorted in chronological order. As per the WSR-88Ds VCP naming convention, those with only two digits are conventional (i.e., not phase coded), and those with three digits have the phase coding technique [2] applied to the CD scan. As expected, it can be seen that the relative number of gates recovered for the conventional scans is generally higher than with phase-coded scans. This is because the phase coding technique recovers large regions with range-overlaid returns, although it leaves circular-shaped artifacts on the data. The mean number of recovered gates with conventional scans is 25.67% and with phase-coded scans is of 12.42%. The recovered areas (in km^2) are provided as an absolute metric to

TABLE I
VRAD ALGORITHM PERFORMANCE SUMMARY

Radar Name	City and State	Date	Time (UTC)	VCP	Samples Rec. (%)	Area Rec. (km^2)	Failed Samples (%)
KDLH	Duluth, MN	16 March 2013	01:11:21	32	24.8%	52,772	<0.01
KCRI	Norman, OK	15 January 2017	20:04:24	21	25.67%	32,749	<0.01
KHGX	Houston, TX	26 August 2017	2:17:36	212	10.24%	19,978	0.02
KILX	Lincoln, IL	22 June 2020	22:03:18	212	6.64%	12,405	0.12
KCRI	Norman, OK	13 December 2020	21:54:49	32	26.55%	37,794	0.03
KTLX	Oklahoma City, OK	29 April 2021	04:24:25	212	15.34%	22,363	0.09
KTLX	Oklahoma City, OK	27 February 2023	03:35:41	212	9.216%	14,077	0.17
KDVN	Quad Cities, IA	01 April 2023	00:36:03	212	11.38%	17,195	0.46
KFDR	Frederick, OK	16 June 2023	00:34:53	212	23.53%	36,973	0.21
KLWX	Sterling, VA	7 August 2023	22:06:21	212	10.56%	14,400	0.65

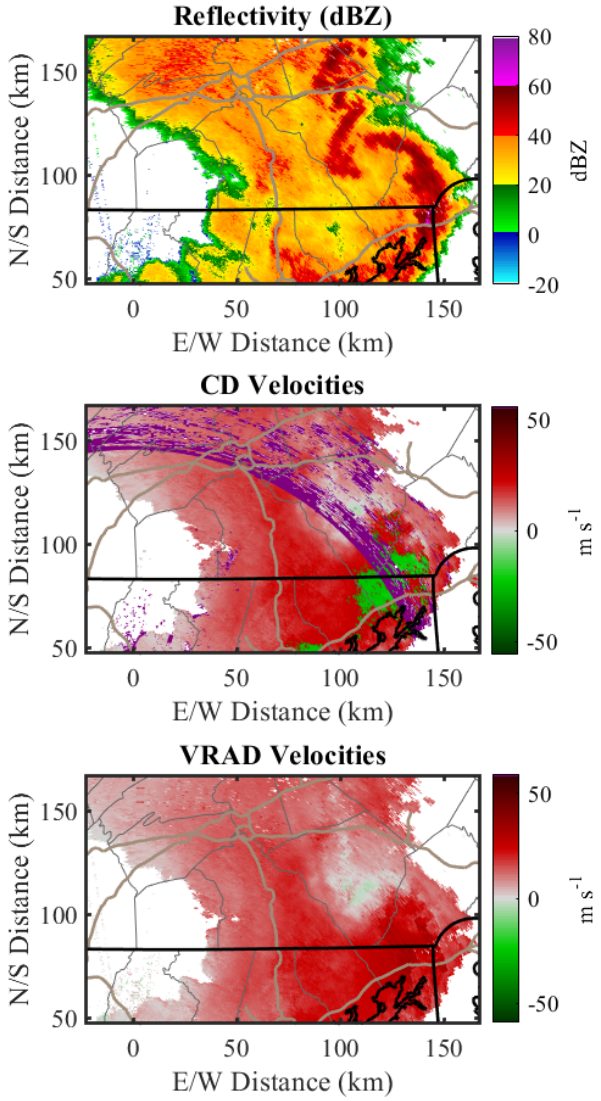

Fig. 10. Same as Fig. 9, but zoomed into the region with range-overlaid returns north-east of the radar.

quantify potential benefits of an operational implementation of this technique. Finally, it can be seen that the dealiasing failure for all cases is on average low, less than 1% of all significant meteorological returns. Higher failures are observed in cases with strong shear (aliasing in the CD scan), especially when it occurs around the regions with range-overlaid returns. These could be mitigated combining this algorithm with other techniques proposed in the literature [22]. Some limitations of the proposed algorithm are discussed next.

The VRAD algorithm can bring important operational benefits to surveillance weather radars; however, some limitations need to be considered. First, dealiasing errors can result in large regions with overlaid returns, and where CD-scan aliasing occurred. When aliasing occurs around regions with overlaid returns, it is challenging to dealias velocities due to the lack of spatial continuity which increases ambiguity. This is hard for any dealiasing algorithm, and potentially could be mitigated by improving the VRAD algorithm or using other more advanced dealiasing concepts [23], [24], [25]. Moreover, this can be exacerbated in the echo recovery using the CS data, since CS-derived velocities may be aliased multiple times (especially if CD velocities are aliased). Next, the velocity difference dealiasing may not be effective for certain pairs of CS/CD PRTs currently used in operational VCPs, especially when PRTs are multiples of one another. That is, there are certain PRT ratios that result in more well-defined velocity differences and minimize dealiasing errors; this has been documented in previous SPRT research [26], [27], [28]. This can be mitigated by making small adjustments to PRTs used to maintain the desired scan parameters while optimizing dealiasing performance. And although the velocity difference dealiasing technique is effective in the VRAD algorithm (which uses median filtering afterward), it may be detrimental in cases of fast-moving storms at close ranges. This is because of the time difference between the CS and CD scans (usually in the order of 20 s). Comparing their velocity fields directly when storms are moving fast (and at close ranges) may be ineffective. To mitigate this, an additional check must be performed prior to the use of velocity difference dealising to evaluate if the velocity fields are in high agreement. This could be done using a simple spatial correlation filter on nonaliased velocity regions or after dealiasing. Note that this would not be a challenge in dual-PRF (or "batch") scans, nor when using emerging phased array radar technology [29]. Finally, although relatively modern processors can apply 2-D median filtering in real time, median calculation can be a computationally intensive operation. Thus, further investigation needs to be conducted to evaluate feasibility for real-time implementation of the VRAD algorithm as is. The average VRAD processing time for the cases in Table I is 28 s (one elevation scan) using

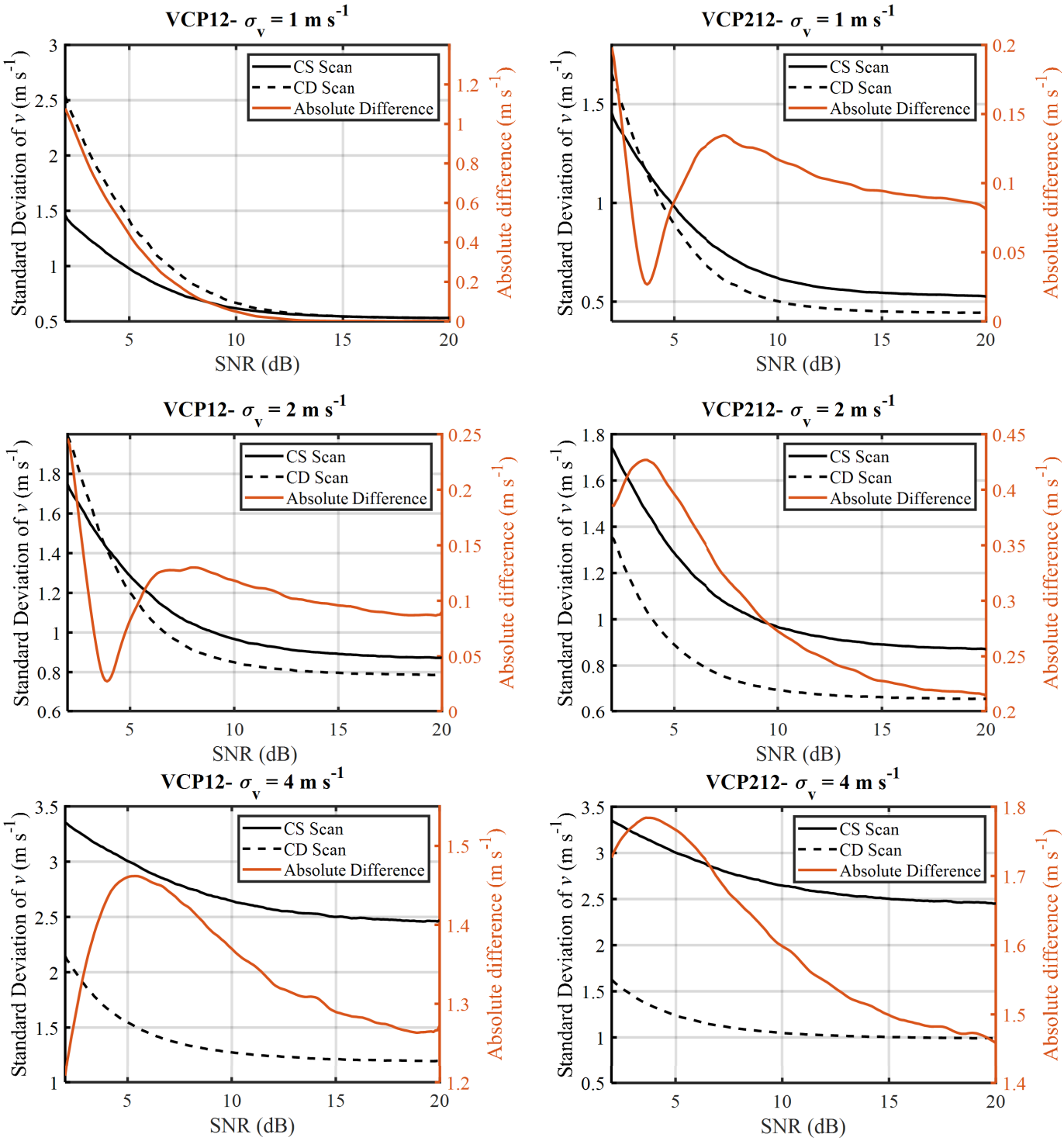

Fig. 11. Standard deviation of simulated Doppler velocity estimates. The left column plots correspond to simulations based on VCP 12 parameters, while those on the right plots correspond to VCP 212 parameters. From top to bottom, the rows present results for different σ_v values, for 1, 2, and 4 ms^{-1}. The Von Hann window was applied to the time-series data to emulate the WSR-88D Doppler velocity processing.

a workstation with the Windows 10 Pro operating system, an AMD Ryzen Threadripper Pro 5975WX central processing unit, and with 128 GB of RAM. The source code was not optimized for efficient or parallel processing. Alternatively, other efficient dealiasing techniques [20], [21] could be used, followed by the echo recovering technique. These open questions are left for future studies.

V. Conclusion

In this study, we introduced a novel Doppler VRAD algorithm designed to address the inherent range–velocity ambiguities present in multi-PRT scans used by weather radars. By leveraging the capabilities of both CS and CD scans, our algorithm significantly enhances spatial extent of

valid Doppler velocity estimates by producing velocity estimates in regions where they did not exist before.

Our algorithm combines simple yet effective dealiasing techniques with a velocity recovery process that exploits the complementary strengths of CS and CD scans. We demonstrated through experimental evaluations, including both conventional and phase-coded scans, that the VRAD algorithm is capable of recovering velocity estimates in areas previously obscured due to aliasing or the presence of range-overlaid returns. This improvement was quantified by a marked increase in the percentage of velocity estimates recovered across various weather events, including severe weather outbreaks and hurricanes.

Furthermore, the algorithm's ability to populate obscured velocity regions with CS scan data while maintaining a smooth transition between CS and CD data is particularly noteworthy. This feature not only enhances the completeness of the velocity fields but also has the potential to provide meteorologists with more reliable data for forecasting and analysis, especially in the context of severe weather events.

While the VRAD algorithm demonstrates a significant advancement in dealing with the Doppler dilemma, we acknowledge certain limitations, including its performance in cases of strong shear or when aliasing occurs around regions with range-overlaid returns. Future work will focus on refining the algorithm to address these challenges, exploring the optimization of PRT ratios, and investigating the feasibility of real-time implementation.

In conclusion, the VRAD algorithm represents a significant step forward in the ongoing effort to improve weather radar capabilities. By increasing the availability of Doppler velocity estimates, this algorithm has the potential to improve interpretation of Doppler velocity fields. The algorithm is directly applicable to operational radars in the United States (NEXRAD); however, any radar system that uses split cuts or dual-PRF scans could implement the algorithm to increase the recovery of Doppler velocity data (e.g., French radar network [30]). Further research and development will continue to refine and adapt this algorithm to meet the evolving needs of meteorological research and operational forecasting.

Future research efforts include a thorough evaluation of the quality of resulting VRAD velocity estimates (i.e., standard deviations), the demonstration of the VRAD algorithm on batch scans, and the evaluation of the algorithm through a time series of volume scans for the same storm. The evaluation of VRAD estimate accuracy could be conducted using valid fields of CD velocities as ground truth and artificially introducing RF regions into these fields. The VRAD algorithm would then be applied to the artificially modified field of CD velocities, and the resulting VRAD velocities recovered would be compared to the true CD velocities. Furthermore, more investigation on how to mitigate the limitations described in Section IV would be important.

ACKNOWLEDGMENT

The authors would like to thank Dr. Dušan Zrnić, Dr. Igor Ivić, and Dr. Jacob Carlin for comments that improved this manuscript. Data was provided by NOAA's National Centers for Environmental Information (NCEI) system.

REFERENCES

[1] M. J. Istok et al., "WSR-88D dual polarization initial operational capabilities," in *Proc. 89th Amer. Meteorological Soc. Annu. Meeting*, 2009, pp. 1–14.

[2] M. Sachidananda and D. S. Zrnic, "Systematic phase codes for resolving range overlaid signals in a Doppler weather radar," *J. Atmos. Ocean. Technol.*, vol. 16, no. 10, pp. 1351–1363, 1999, doi: 10.1175/1520-0426(1999)016<1351:SPCFRR>2.0.CO;2.

[3] D. Schvartzman, S. M. Torres, and D. Warde, "The hybrid-scan estimators: Exploiting WSR-88D split cuts to improve the quality of polarimetric-variable estimates," *J. Atmos. Ocean. Technol.*, vol. 37, no. 2, pp. 299–315, Feb. 2020.

[4] R. J. Doviak and D. Zrnic, *Doppler Radar and Weather Observations*. Mineola, NY, USA: Dover, 2006.

[5] Office of the Federal Coordinator for Meteorological Services and Supporting Research (OFCM). (2006). *WSR-88D unit description Operational applications. Part D, Doppler Radar Meteorological Observations*. US Department of Commerce/NOAA. [Online]. Available: https://www.ofcm.gov/publications/fmh/FMH11/FMH11D-2006.pdf

[6] Office of the Federal Coordinator for Meteorological Services and Supporting Research (OFCM). (2017). *WSR-88D Products and Algorithms. Part C, WSR-88D Meteorological Observations, Federal Meteorological Handbook*. US Department of Commerce/NOAA. [Online]. Available: https://www.ofcm.gov/publications/fmh/FMH11/fmh11partC.pdf

[7] R. J. Keeler and R. E. Passarelli, *Signal Processing for Atmospheric Radars*. Boston, MA, USA: American Meteorological Society, 1990, pp. 199–229, doi: 10.1007/978-1-935704-15-7_21.

[8] I. Holleman and H. Beekhuis, "Analysis and correction of dual PRF velocity data," *J. Atmos. Ocean. Technol.*, vol. 20, no. 4, pp. 443–453, 2003. [Online]. Available: https://journals.ametsoc.org/view/journals/atot/20/4/1520-0426_2003_20_443_aacodp_2_0_co_2.xml

[9] W. D. Zittel, D. Saxion, R. Rhoton, and D. C. Crauder, "P2. 9 combined WSR-88D technique to reduce range aliasing using phase coding and multiple Doppler scans," in *Proc. 88th Amer. Meteorological Soc. Annu. Meeting*, 2008, pp. 1–10.

[10] A. Losey-Bailor, W. D. Zittel, and Z. Jing, "3–25 improving Doppler velocity coverage on the WSR-88D by using low PRFs with 2DVDA," in *Proc. 39th Int. Conf. Radar Meteorol.*, 2019, pp. 1–9.

[11] D. A. Warde, A. Heck, J. Krause, A. Losey, and W. D. Zittel, "828 A novel approach to reducing dealiasing errors for staggered pulse repetition time waveforms," in *Proc. 99th Amer. Meteorological Soc. Annu. Meeting*, 2019, pp. 1–6.

[12] S. M. Torres, Y. F. Dubel, and D. S. Zrn, "Design, implementation, and demonstration of a staggered PRT algorithm for the WSR-88D," *J. Atmos. Ocean. Technol.*, vol. 21, no. 9, pp. 1389–1399, 2004. [Online]. Available: https://journals.ametsoc.org/view/journals/atot/21/9/1520-0426_2004_021_1389_diadoa_2_0_co_2.xml

[13] W. D. Zittel, Z. Jing, and R. O. Center, "Comparison of a 2-D velocity dealiasing algorithm to the legacy WSR-88D velocity dealiasing algorithm during Hurricane Irene," in *Proc. 30th Conf. Hurricanes Tropical Meteorol.*, 2012, pp. 1–8.

[14] S. M. Torres and D. A. Warde, "Staggered-PRT sequences for Doppler weather radars. Part I: Spectral analysis using the autocorrelation spectral density," *J. Atmos. Ocean. Technol.*, vol. 34, no. 1, pp. 51–63, 2017. [Online]. Available: https://journals.ametsoc.org/view/journals/atot/34/1/jtech-d-16-0071.1.xml

[15] D. Zrni and D. Schvartzman, "Phase codes for mitigating ambiguities in range and velocity," *J. Atmos. Ocean. Technol.*, vol. 38, no. 2, pp. 313–329, 2021. [Online]. Available: https://journals.ametsoc.org/view/journals/atot/38/2/JTECH-D-20-0131.1.xml

[16] D. S. Zrnić, "Simulation of weatherlike Doppler spectra and signals," *J. Appl. Meteorol.*, vol. 14, no. 4, pp. 619–620, Jun. 1975. [Online]. Available: https://journals.ametsoc.org/view/journals/apme/14/4/1520-0450_1975_014_0619_sowdsa_2_0_co_2.xml

[17] L. M. Richardson and I. R. Ivić, "A less-tapered signal processing window for polarimetric variables," in *Proc. 39th Int. Conf. Radar Meteorol.*, 2019, pp. 1–9.

[18] M. Fang, R. J. Doviak, and V. Melnikov, "Spectrum width measured by WSR-88D: Error sources and statistics of various weather phenomena," *J. Atmos. Ocean. Technol.*, vol. 21, no. 6, pp. 888–904, 2004. [Online]. Available: https://journals.ametsoc.org/view/journals/atot/21/6/1520-0426_2004_021_0888_swmbwe_2_0_co_2.xml

[19] S. M. Torres and D. S. Zrni, "Whitening of signals in range to improve estimates of polarimetric variables," *J. Atmos. Ocean. Technol.*, vol. 20, no. 12, pp. 1776–1789, 2003. [Online]. Available: https://journals.ametsoc.org/view/journals/atot/20/12/1520-0426_2003_020_1776_wosirt_2_0_co_2.xml

[20] H. Kim and B. Cheong, "Robust velocity dealiasing for weather radar based on convolutional neural networks," *Remote Sens.*, vol. 15, no. 3, p. 802, 2023.

[21] M. S. Veillette, J. M. Kurdzo, P. M. Stepanian, J. McDonald, S. Samsi, and J. Y. N. Cho, "A deep learning-based velocity dealiasing algorithm derived from the WSR-88D open radar product generator," *Artif. Intell. Earth Syst.*, vol. 2, no. 3, 2023, Art. no. e220084. [Online]. Available: https://journals.ametsoc.org/view/journals/aies/2/3/AIES-D-22-0084.1.xml

[22] A. A. Alford, M. I. Biggerstaff, C. L. Ziegler, D. P. Jorgensen, and G. D. Carrie, "A method for correcting staggered pulse repetition time (PRT) and dual pulse repetition frequency (PRF) processor errors in research radar datasets," *J. Atmos. Ocean. Technol.*, vol. 39, no. 11, pp. 1763–1780, Nov. 2022.

[23] S. Muth, S. Dort, I. A. Sebag, M.-J. Blais, and D. Garcia, "Unsupervised dealiasing and denoising of color-Doppler data," *Med. Image Anal.*, vol. 15, no. 4, pp. 577–588, Aug. 2011. [Online]. Available: https://www.sciencedirect.com/science/article/pii/S1361841511000454

[24] V. Louf, A. Protat, R. C. Jackson, S. M. Collis, and J. Helmus, "UNRAVEL: A robust modular velocity dealiasing technique for Doppler radar," *J. Atmos. Ocean. Technol.*, vol. 37, no. 5, pp. 741–758, May 2020.

[25] A. Protat, V. Louf, and M. Curtis, "A novel Doppler unfolding technique using optical flow," *J. Atmos. Ocean. Technol.*, vol. 40, no. 10, pp. 1263–1276, Oct. 2023. [Online]. Available: https://journals.ametsoc.org/view/journals/atot/40/10/JTECH-D-23-0057.1.xml

[26] Y. Golestani, V. Chandrasekar, and R. J. Keeler, "Dual polarized staggered PRT scheme for weather radars: Analysis and applications," *IEEE Trans. Geosci. Remote Sens.*, vol. 33, no. 2, pp. 239–246, Mar. 1995.

[27] M. Sachidananda and D. S. Zrni, "Clutter filtering and spectral moment estimation for Doppler weather radars using staggered pulse repetition time (PRT)," *J. Atmos. Ocean. Technol.*, vol. 17, no. 3, pp. 323–331, 2000. [Online]. Available: https://journals.ametsoc.org/view/journals/atot/17/3/1520-0426_2000_017_0323_cfasme_2_0_co_2.xml

[28] P. Tabary, L. Perier, J. Gagneux, and J. P. D. Chatelet, "Test of a staggered PRT scheme for the French radar network," *J. Atmos. Ocean. Technol.*, vol. 22, no. 4, pp. 352–364, 2005. [Online]. Available: https://journals.ametsoc.org/view/journals/atot/22/4/jtech1709_1.xml

[29] R. Palmer et al., "A primer on phased array radar technology for the atmospheric sciences," *Bull. Amer. Meteorological Soc.*, vol. 103, no. 10, pp. 2391–2416, 2022.

[30] P. Tabary, F. Guibert, L. Perier, and J. P. D. Chatelet, "An operational triple-PRT Doppler scheme for the French radar network," *J. Atmos. Ocean. Technol.*, vol. 23, no. 12, pp. 1645–1656, 2006. [Online]. Available: https://journals.ametsoc.org/view/journals/atot/23/12/jtech1923_1.xml

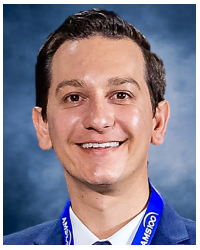

David Schvartzman (Senior Member, IEEE) was born in Piracicaba, Brazil, on March 17, 1988. He received the B.S. degree in electrical and computer engineering from the National University of Asunción, San Lorenzo, Paraguay, in 2011, and the M.S. and Ph.D. degrees in electrical and computer engineering from the University of Oklahoma, Norman, OK, USA, in 2015 and 2020, respectively.

From 2015 to 2020, he was a Research Scientist with the NOAA National Severe Storms Laboratory (NSSL) and the Cooperative Institute for Severe and High-Impact Weather Research and Operations (CIWRO). From 2021 to mid-2022, he was a Research Scientist with the Advanced Radar Research Center (ARRC), The University of Oklahoma, where he is currently an Assistant Professor with the School of Meteorology, affiliated with the ARRC and also an Adjunct Assistant Professor with the School of Electrical and Computer Engineering. He works on novel signal and array processing algorithms to improve understanding of atmospheric processes using phased array radar. He also works on calibration and integration of phased array radar systems.

Dr. Schvartzman is a member of the American Meteorological Society (AMS). He was a recipient of the 2023 IEEE R5 *Outstanding Young Professional* Award and the 2019 American Meteorological Society's *Spiros G. Geotis* Prize.

Robert D. Palmer (Fellow, IEEE) was born in Fort Benning, GA, USA, on June 3, 1962. He received the Ph.D. degree in electrical engineering from the University of Oklahoma (OU), Norman, OK, USA, in 1989.

From 1989 to 1991, he was a JSPS Postdoctoral Fellow with the Radio Atmospheric Science Center, Kyoto University, Kyoto, Japan, where his major accomplishment was the development of novel interferometric radar techniques for studies on atmospheric turbulent layers. After his stay in Japan, he was with the Physics and Astronomy Department, Clemson University, Clemson, SC, USA. From 1993 to 2004, he was a part of the faculty of the Department of Electrical Engineering, University of Nebraska–Lincoln, Lincoln, NE, USA, where his interests broadened into areas including wireless communications, remote sensing, and pedagogy. Soon after moving to OU as the Tommy C. Craighead Chair at the School of Meteorology in 2004, he established the interdisciplinary Advanced Radar Research Center (ARRC). He currently serves as the Executive Director of the ARRC and OU's Associate Vice President for Research and Partnerships. While at OU, his research interests have focused on the application of advanced radar signal processing techniques to observations of severe weather, particularly related to phased array radars and other innovative system designs. He has published widely in the area of radar sensing of the atmosphere, with more than 125 peer-reviewed journal articles, one textbook, 50 international invited talks, and hundreds of conference presentations.

Prof. Palmer is a fellow of the American Meteorological Society (AMS) and the Institute of Electrical and Electronics Engineers (IEEE) emphasizing his dedication to the interdisciplinary nature of radar science.